

# **Needle Deflection and Path Correction for Printing in Liquid Like Solids**

**Wyatt Ebert  
Summa Cum Laude  
Spring 2018**

# Needle Deflection and Path Correction for Printing in Liquid like Solids

W. Ebert • A. McGhee • S. Niemi

**Abstract** Printing 3D structures into a continuum of jammed microgel particles is a recent development showing great promise for the development of regenerative medicine. The deposition of material into the microgel support medium has shown the ability to generate structures with feature sizes less than 100  $\mu\text{m}$  (Christopher S. O'Bryan, 2017). For these detailed structures, it is essential to quantify the effects the support medium may have on printing precision. A series of tests are conducted to investigate the needle deflection and needle recovery on right angle geometries. Printing over a range of 3 orders of magnitude in sliding speed, needle deflections were measured to be approximately 0.58 mm regardless of speed. The recovery distance of the deflection was also seen to be speed independent. An iterative method for path correction to achieve the target right angle geometry is proposed.

## Introduction

The recent development of 3D printing soft structures into a continuum of jammed microgel particles has shown significant capabilities for use in regenerative medicine. The needle of a syringe moves through the microgel while extruding a print material. The print material is held in place by the microgel, allowing full structures to be created. The pressures from the microgel acting on the submerged length of the needle cause inherent deflections at the tip of the needle.

A recent study explores needle bending in these microgels by quantifying tip deflections for a spread of needle dimensions and print velocities while moving in a linear motion (A. McGheeEmail, 2018). This study begins to explore how needle bending will affect the precision of printing distinct features. The feature chosen to analyze is a right angle, due to its infinitely small radius. Right angles are printed over a sweep of velocities. The needle tip paths are quantified to determine the deviation from the target right angle. Correction paths are proposed to result in a needle tip path closer to the target right angle.

## **Materials and Method**

### *Support Medium Preparation*

The features are printed into a jammed microgel support medium. The microgel samples are prepared by dispersing Ashland 980 dry carbomer powder in ultrapure water (Millipore, 18 M $\Omega$ ) at a concentration of 7.5 % (w/w). Batches of the carbomer-water solution were mixed using a centrifugal speed mixer at 3500 rpm for 15 min. The concentrated solution was then diluted into a larger container to the desired 0.2% concentration. The microgel solution was swollen through the addition of 5 mL of a 1 molar sodium hydroxide (NaOH) solution per gram of dry carbomer. The solution is mixed in a closed container and allowed to equilibrate for a minimum of 24 hours to ensure homogeneity.

### *Printing Material Preparation*

The features are printed with a mixture of microgel and black paint. A 0.1% (w/w) microgel sample is prepared (see *support medium preparation*). Three drops of black acrylic paint are added to 20 ml of the 0.1% microgel. The paint-microgel solution is mixed using a centrifugal speed mixer at 2500 rpm for 30 s to ensure a homogenous black color.

### *Experimental Set Up*

Small portions of the 0.2% microgel are mixed in a centrifugal speed mixer at 2500 rpm for 30s to remove air bubbles. The microgel is then poured into a 100 mm diameter, clear, plastic, flat bottom dish such that the surface of the microgel is protruding above the top edge of the dish. Any newly trapped air bubbles are removed using a pipette. A rigid, flat edged, tool is swept across the top edge of the dish, removing the microgel protruding above the top edge, resulting in a flat microgel surface, which is level with the top edge of the dish. The flattened surface and removal of air bubbles allows a uniform submerged needle tip depth while printing and a high contrast image to be taken, free of additional glare and shadows caused by an uneven microgel surface (see *Figure 1*).



Figure 1: clear dish filled with microgel and air bubbles removed (left); surface leveled (right)

The 0.2% microgel sample is placed on a clear and level glass table. A camera is supported under the glass table, such that the lens is 15 cm below the bottom of the microgel sample. The camera (Basler acA640-120  $\mu\text{m}$ ) and lens (Computar 12 – 36 mm 1:2.8) are leveled before printing.

A 1 ml syringe is filled with the black 0.1% microgel. The needle attached to the syringe is stainless steel with a 39.45 mm length, 0.41 mm outer diameter, and 0.21 mm inner diameter. The syringe is attached to a 3D printer consisting of 3 linear actuation stages, corresponding to X, Y, and Z axes. The stages (Newport High Performance ILS Linear Stages, Stepper Motor, Metric) have corresponding travel lengths 300 mm, 200 mm, and 200 mm. X and Y stages are aligned with the horizontal plane and Z stage with the vertical direction. Features are printed over a range of velocities with predetermined flow rate settings. Flow rates are set to achieve features that are thin while remaining continuous.

The needle tip is centered above the camera and corresponding X and Y stage positions are recorded. The starting position of the print is set such that the vertex of the right-angle will lie centered above the camera's field of view to minimize effects of the curved lens on the image taken. The needle tip is positioned above the 0.2% microgel sample and lowered until contacting the top surface. This Z position is recorded and implemented into the printing path such that the right-angle is printed with the needle tip submerged 10 mm in the microgel sample.

With the microgel sample roughly centered above the camera, the printer executes a right-angle by moving 20 mm in the (+)X direction, to a position centered above the camera's field of view, then instantly moves 25 mm in the (+)Y direction. The needle is moved away from the sample, while keeping the sample in its original position. A white backdrop, with highly diffused light source is placed over the sample, while keeping the sample in its original position. An image of the printed feature is taken (see *Figure 2*). High contrasts between the black feature and white backdrop is important for the analysis of the image. If adjustments to the camera's settings are made to achieve an image with desired contrast, the camera is re-leveled, needle tip re-aligned with the camera's field of view, and print completed a second time.

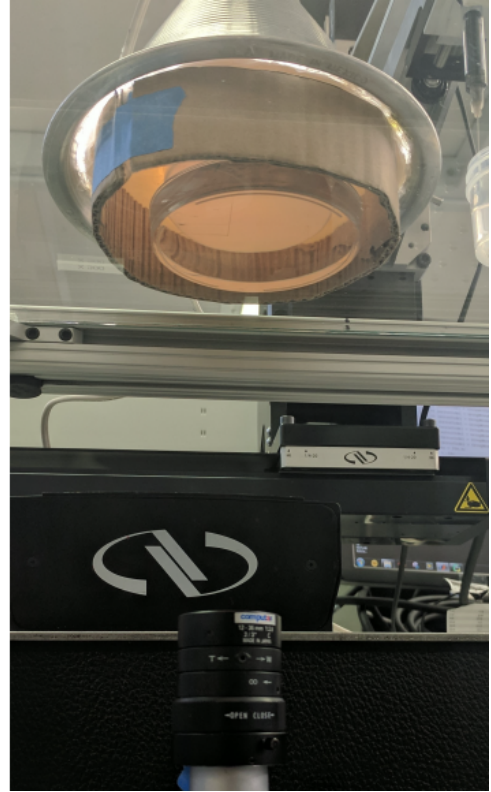


Figure 2: feature printed (left); lighting adjusted, and image taken (right)

An image is taken with the needle tip submerged to the 10 mm depth and positioned 5 mm in the (+)X direction from the camera's center. The needle tip is then, raised out of the sample, moved 10 mm in the (-)X direction, re-lowered to a 10 mm depth and imaged. These two images, with needle tips 5 mm off center in opposite directions are used to determine the pixel to mm scaling factor for the images of the right-angle prints.

### Image Analysis Via MATLAB

A MATLAB code is written to quantify the path of the needle tip during each print. The high contrast images (see *Figure 3*) are uploaded to MATLAB as a matrix of intensity values. Each position of the matrix corresponds to a pixel of the original image and the numeric value in each position represents the light intensity of each pixel. Intensity values range from 0 to 255. High intensity values correspond to brighter pixels, while the lower intensity values correspond to darker pixels. When plotted as 3D contours in MATLAB, high intensity values of the white background are shown as shades of yellow, while the black printed features as shades of blue and purple. The basis of the code relies on the assumption that the locations of the lowest intensity values and darkest pixels of the image would correspond to the middle of the lines being printed, and therefore the path of, specifically, the center of the needle tip.

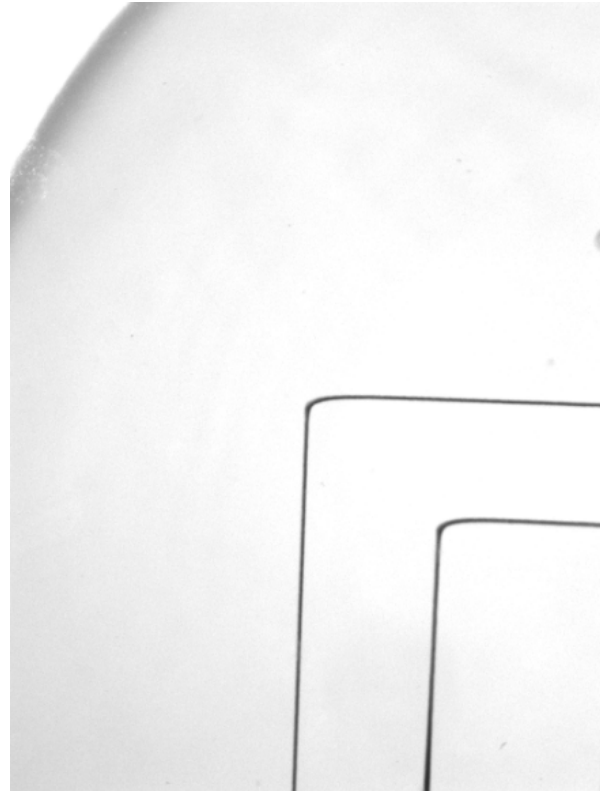


Figure 3: high contrast image of printed feature

Once the image is uploaded as an intensity plot it is cropped and a threshold applied (see *Figure 4*). The threshold sets the background to a constant value of 250 while preserving the intensity values of the printed feature. The X and Y stages of the printer are not perfectly aligned with the rows and columns of the pixels of the image. Therefore, a rotation correction is applied. Referring to the print as 2 separate legs in the order they are printed, the image is straightened by referencing a section of the 1<sup>st</sup> leg. The result of the rotation correction is a purely vertical 1<sup>st</sup> leg. The code starts at the 10<sup>th</sup> row and moves up until reaching a user defined row that is close to but before the region where the needle tip begins transitioning into the second leg. For each row, the column location of the minimum intensity value is stored in a matrix, LEG1. Once iterating through the section of rows, the standard deviation of the values within the matrix, LEG1, is stored as the 1<sup>st</sup> value in a second matrix, STDV. The code then rotates the image 0.01 degrees, recalculates the values stored in matrix LEG1, and stores the new standard deviation of LEG1 in the 2<sup>nd</sup> position of STDV. The STDV matrix is filled throughout a range of degrees, which the straightest position of the image will lie. The minimum value in matrix STDV corresponds to a rotation where the first leg is purely vertical. Shown in *Figure 5*, the image is rotated from -1 to -3 degrees, reading right to left. The standard deviation decreases as the image reaches its straightest position (see *Figure 6*). After which, the image begins to over rotate, shown by the increase in standard deviation. The variation of the column positions of the 1<sup>st</sup> leg, in the straightened position are plotted as a visual check, shown in *Figure 7*.

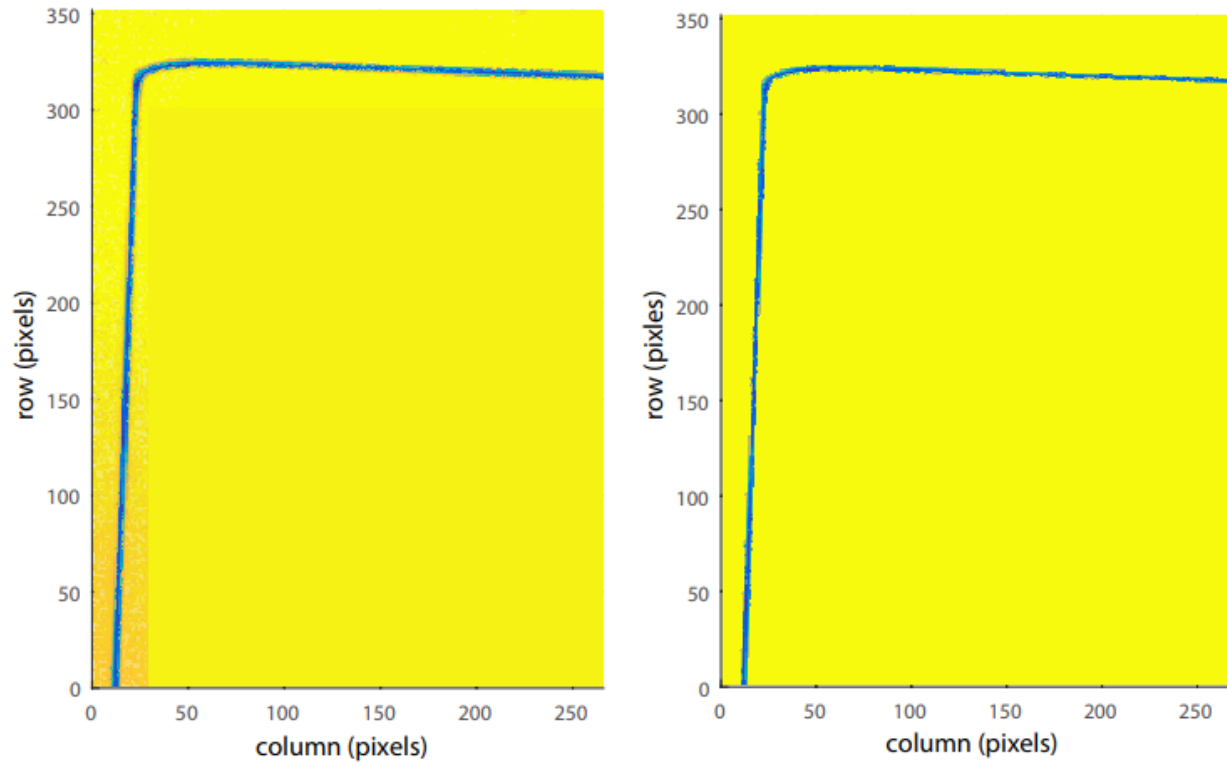


Figure 4: intensity matrix cropped (left); threshold applied (right)

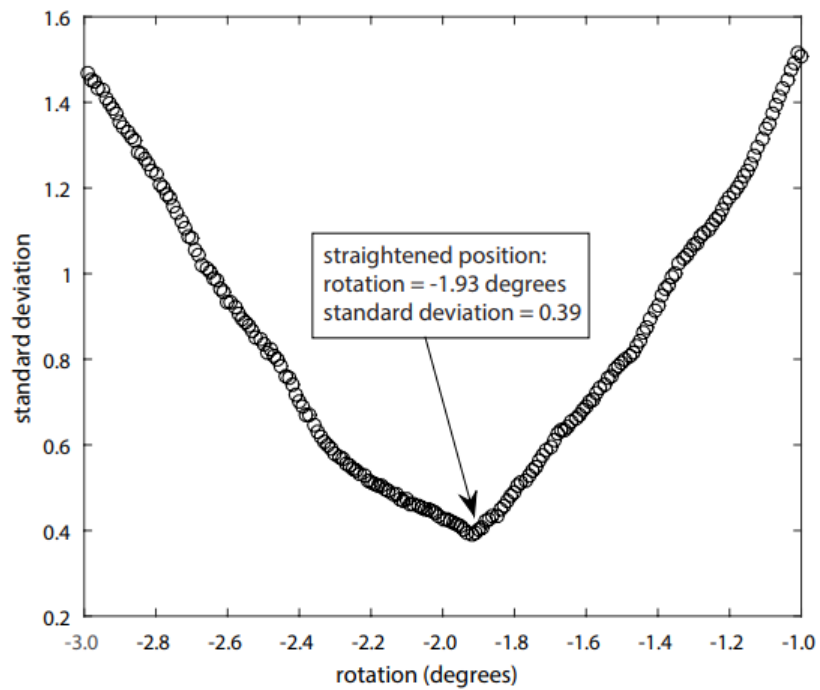


Figure 5: standard deviation of leg 1 positions from rotations -1.0 to -3.0 degrees

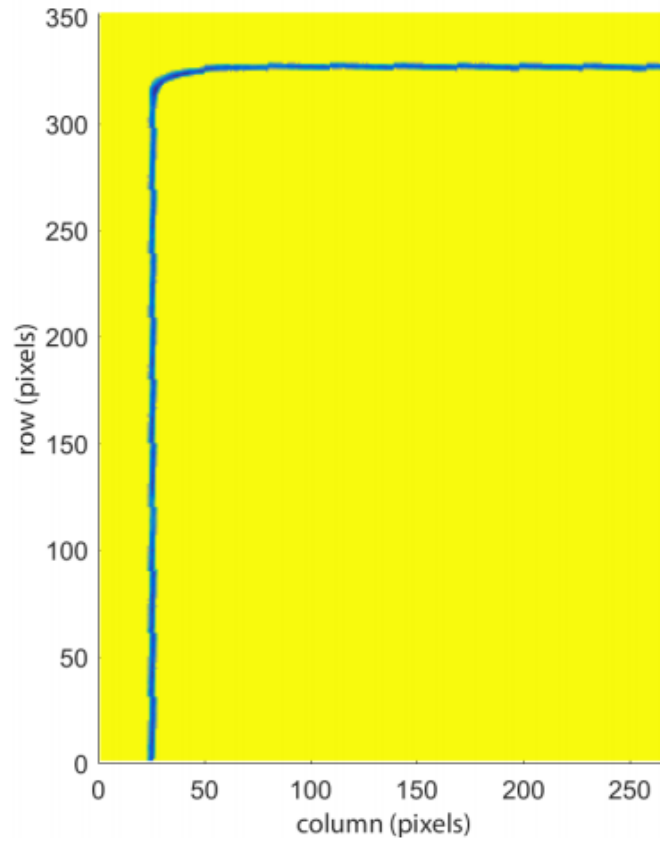


Figure 6: straightened image

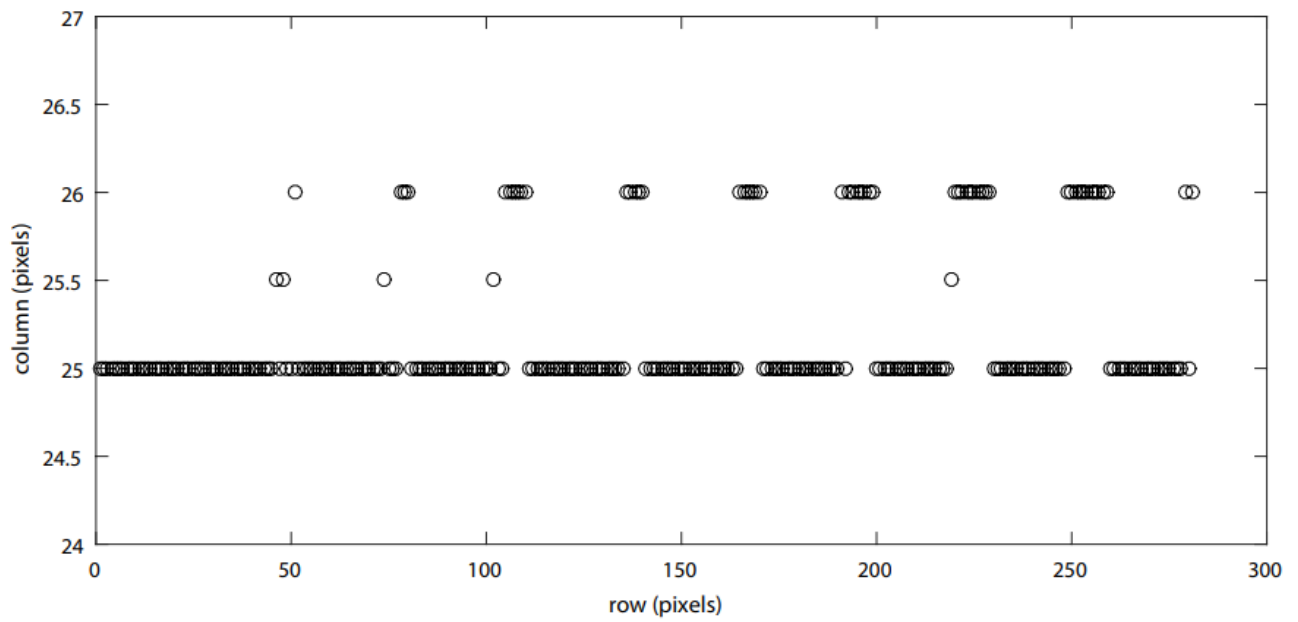


Figure 7: leg 1 column position variation of straightened image

The code then moves through a range of columns to solve the path of the 2<sup>nd</sup> leg. To capture the entire transition from the 1<sup>st</sup> to 2<sup>nd</sup> leg, the 1<sup>st</sup> column analyzed is one position to the right of the most positive column position of the 1<sup>st</sup> leg. Shown in *Figure 7*, the columns corresponding to the location of the 1<sup>st</sup> leg vary between 25 and 26. Therefore, when solving the path of the second leg the code starts at column 27 and ends with the column 15 places before the right edge of the image. For each column, the row location of the minimum intensity value is stored in the matrix, LEG2. The needle tip path throughout the 2<sup>nd</sup> leg can be shown by plotting the values of LEG2, shown in *Figure 8*. Using the scaling factor (see *materials and method*) the results can be scaled from units of pixel locations to mm (see *Figure 9*).

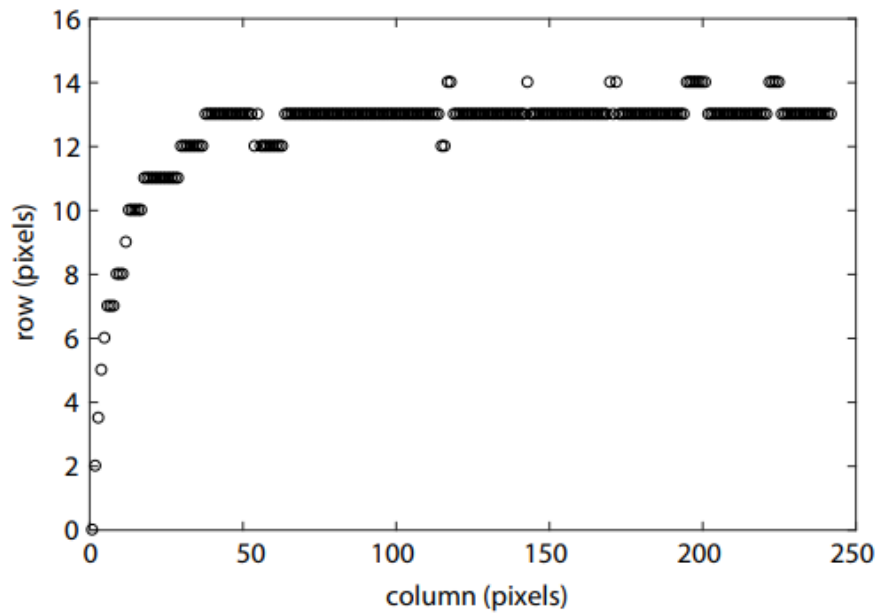


Figure 8: path of 2<sup>nd</sup> leg as pixel locations

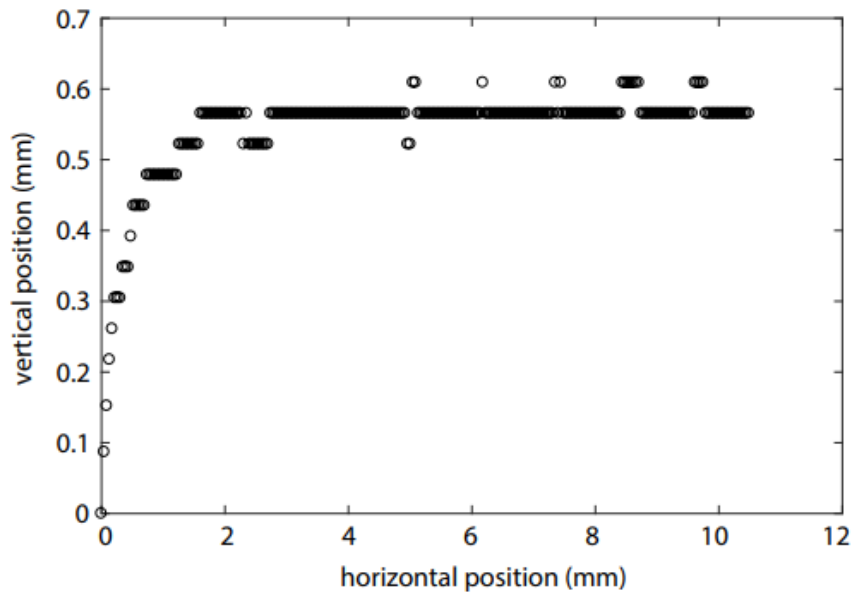


Figure 9: path of 2<sup>nd</sup> leg scaled to mm

The last section of the code provides a visual check of the assumption that the darkest pixels would correspond to the middle of the feature, and therefore the middle of the needle tip's path. Using the straightened intensity matrix, the locations corresponding to the feature were set to values of (1/0). This creates a stencil of the features entire shape, allowing the solved path to be overlaid and clearly visible (see *Figure 10*). Zooming in to the second leg the solved path falls roughly in the middle of the feature, showing the assumption to be safe (see *Figure 11*).

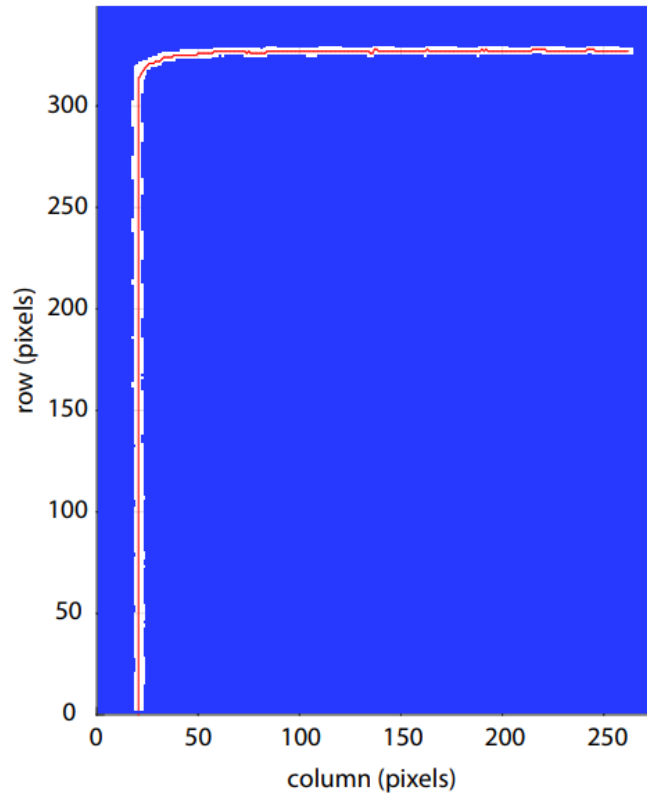


Figure 10: feature outline overlaid with solved needle tip path

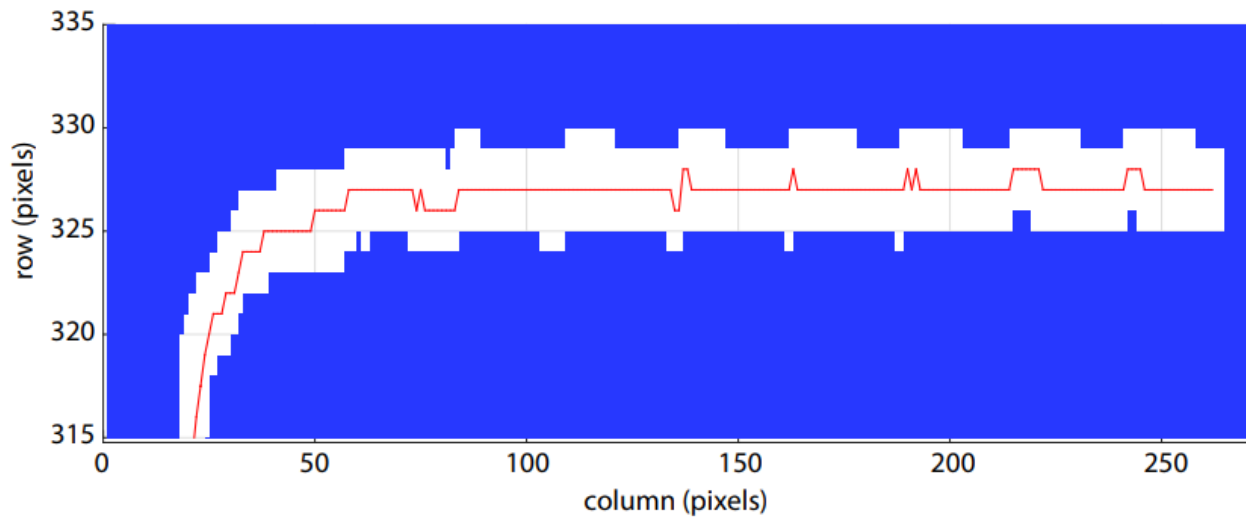


Figure 11: feature outline overlaid with solved needle tip path zoomed to 2<sup>nd</sup> leg

## False Results from Off Center Camera Position

The importance of aligning the vertex of the right angle with the center of the camera's field of view was first noticed during the development of the procedure. To maximize zoom, while capturing a majority of the 2<sup>nd</sup> leg, the camera was positioned as shown in *Figure 12*. After rotating the image to its straightest position, you can see the effects of the curved lens by plotting the column positions of the 1<sup>st</sup> leg. Shown in *Figure 13*, note that this is the same plot as *Figure 7*, with the only difference that the image is taken with a camera position off-center from the vertex of the right angle. The steady bow in the 1<sup>st</sup> leg is a clear indication of the curved lens effects. A similar effect is seen in the 2<sup>nd</sup> leg. Shown in *Figure 14*, a false representation of the 2<sup>nd</sup> leg is solved for.

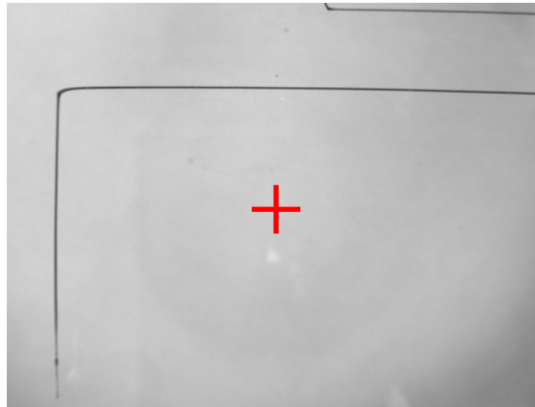


Figure 12: image taken with off-center camera position; center of camera's field of view shown in red

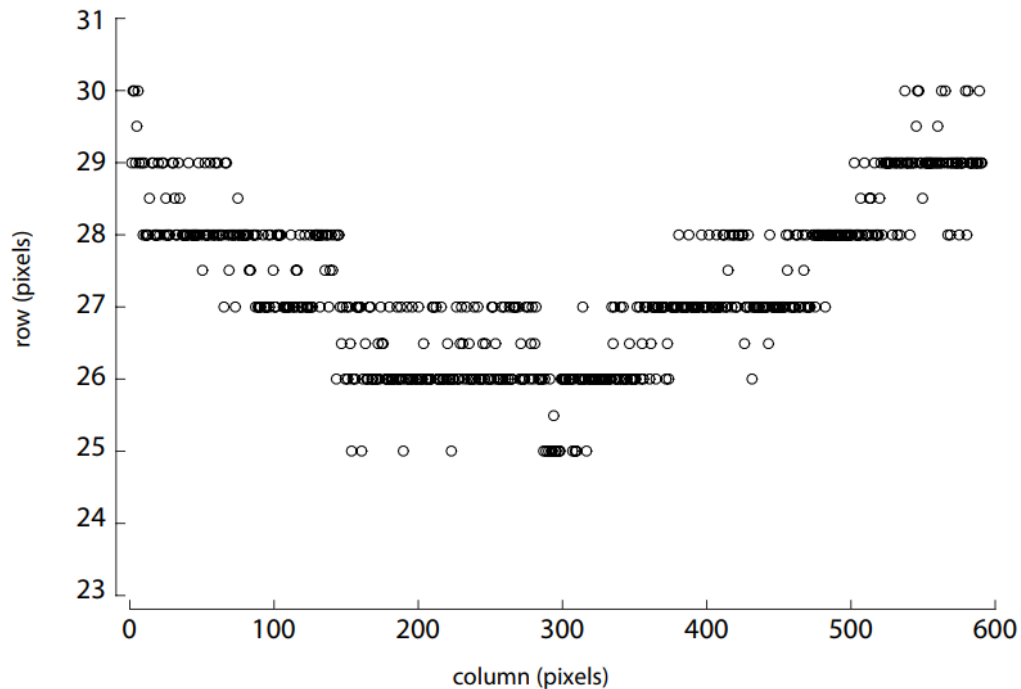


Figure 13: leg 1 column position variation of straightened image with off-center camera position

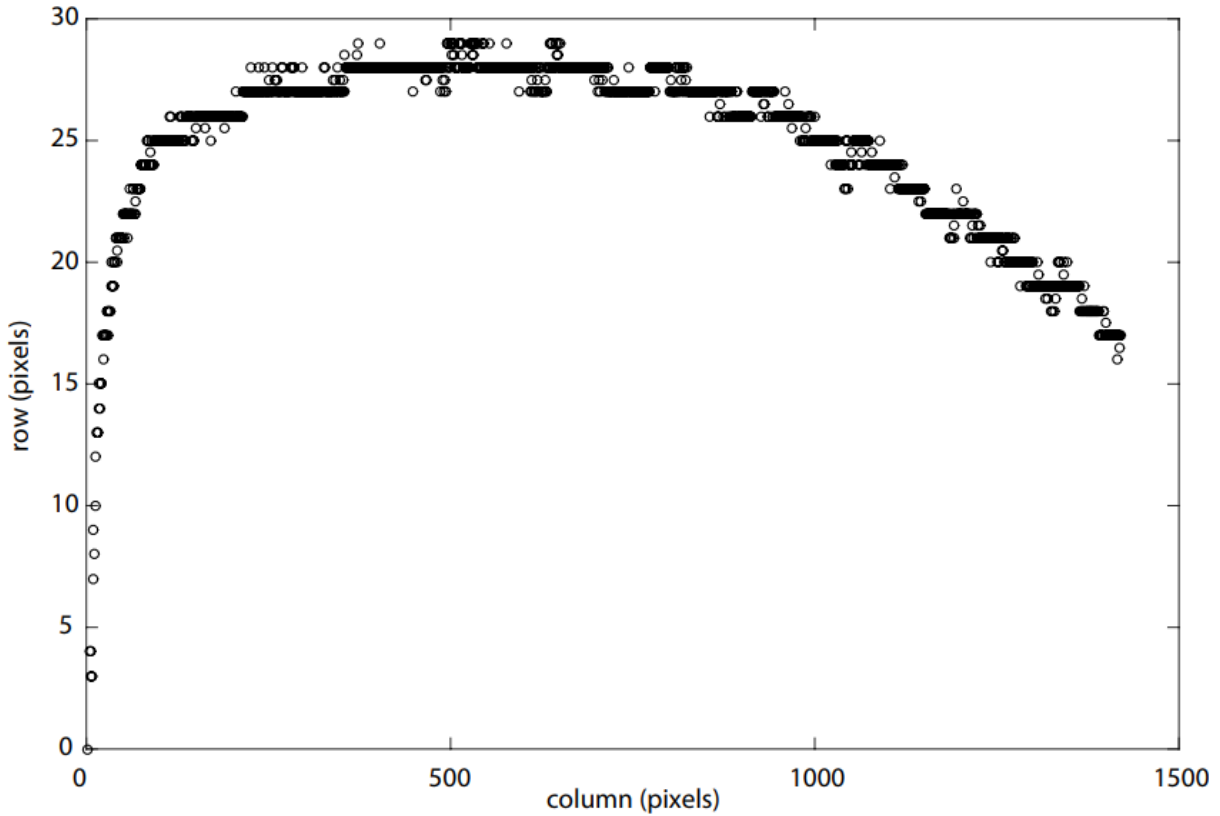


Figure 14: false leg 2 path solved for from image with off-center camera position

### Right Angle Path Results

The individual and average paths of the 2<sup>nd</sup> legs for the 9 prints completed at 1 mm/s are shown in *Figure 15*. The paths are normalized to an average asymptote height. The spread of asymptotes is approximately 0.1 mm. An additional 8 velocities were tested: 0.1, 0.3, 0.5, 3, 5, 10, 30, and 50 mm/s. The individual and average paths of the 2<sup>nd</sup> legs for these velocities are shown in *Figure 16*. Like the 1 mm/s prints, the paths are normalized to an average asymptote height and show extremely close results to the 1 mm/s prints. The average paths of both data sets are overlaid in *Figure 17*. The average asymptote all 17 prints, 0.58 mm, is plotted as the target path.

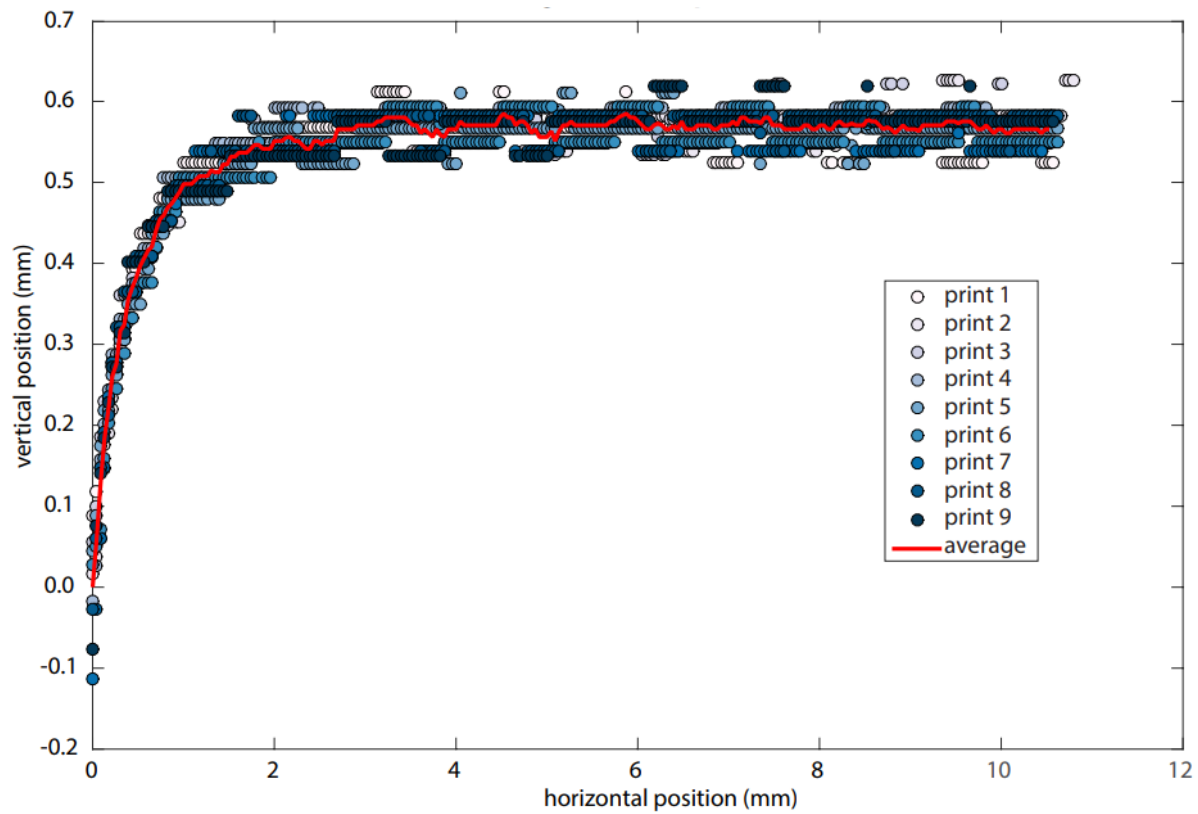


Figure 15: individual and average paths of the 2<sup>nd</sup> legs printed with 1 mm/s velocities

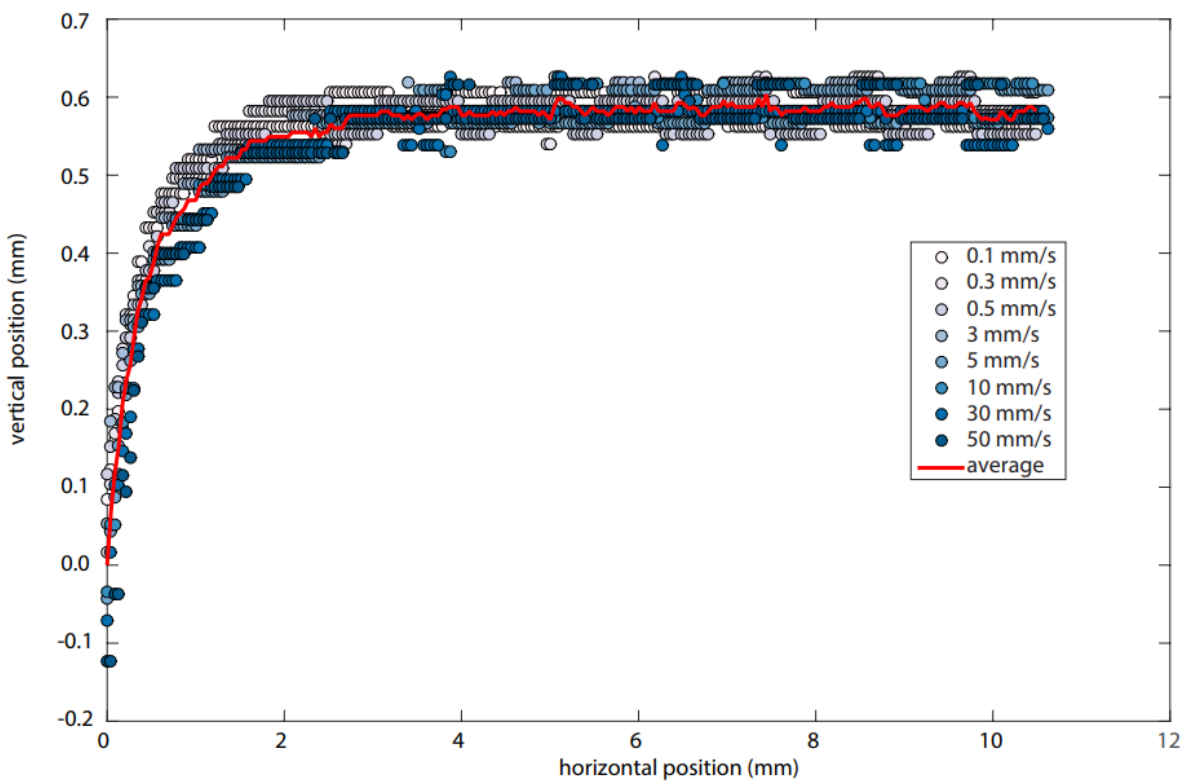


Figure 16: individual and average paths of the 2<sup>nd</sup> legs printed over a range of velocities excluding 1 mm/s

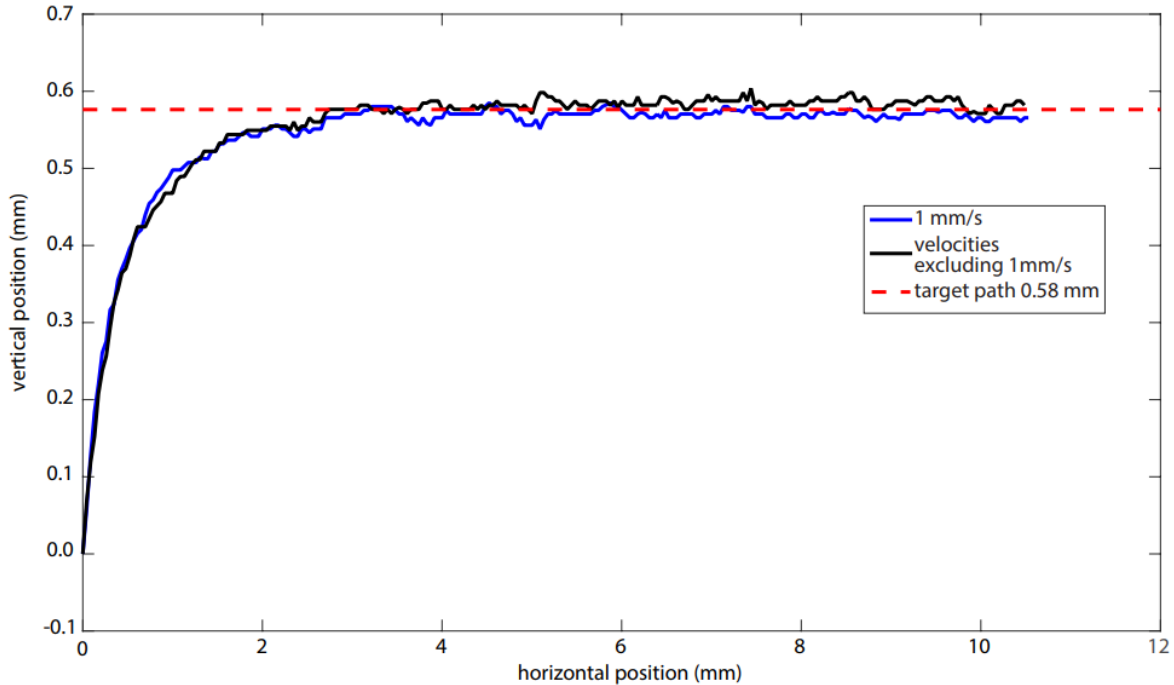


Figure 17: average paths of 2<sup>nd</sup> leg from prints at 1mm/s and prints at velocities excluding 1 mm/s

### Correction Path Generation and Procedure

The results from the right-angle prints are used to generate correction paths. The correction paths overshoot the 2<sup>nd</sup> leg of the right angle through various trajectories. These trajectories are programmed into the printer to force the needle tip to more closely follow the path of a right angle. Due to the similarity in results across all velocities in the right-angle test, the correction paths are tested at a constant 1 mm/s.

The initial correction path, referred to as the full inverse, is generated by flipping the average 2<sup>nd</sup> leg path from the right-angle tests completed at 1 mm/s. The logic is that if the needle is undershooting by a certain vertical distance at a corresponding horizontal location, then overshooting the printer by the equivalent vertical distance at the same horizontal locations should give a result close to the target path. Once the path was flipped and asymptote normalized to 0 (see *Figure 18*), a 2-term exponential function was fit to the that data (see *Figure 19*). A new trajectory file is created by evaluating the fit in 0.005 mm increments from 0 to 4 mm. Because this trajectory is only set to correct the transition region between the 1<sup>st</sup> and 2<sup>nd</sup> legs, the trajectory is extended through a horizontal path until reaching a total horizontal distance of 25 mm. The trajectory is adjusted such that the horizontal and vertical positions correspond to the X and Y stages of the printer, respectively. The new path programmed into the printer consists of moving 20 mm in the (+)Y direction, before instantly executing the correction trajectory. The same procedure completed for the right-angle test is followed. Because the printer is no longer following the path of a right angle, the vertex of the target path is centered above the camera's field of view.

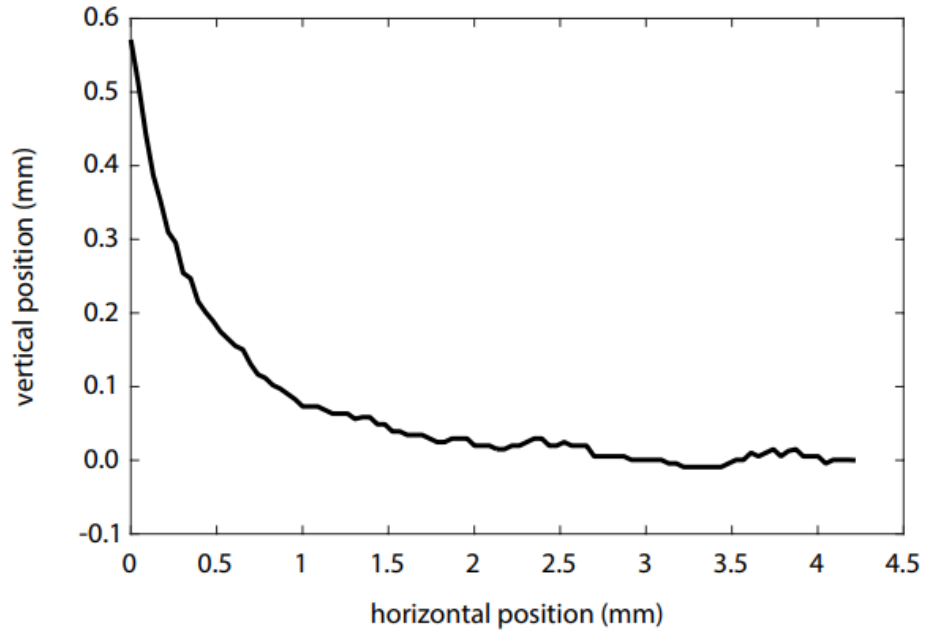


Figure 18: flipped average leg 2 path of prints at 1 mm/s

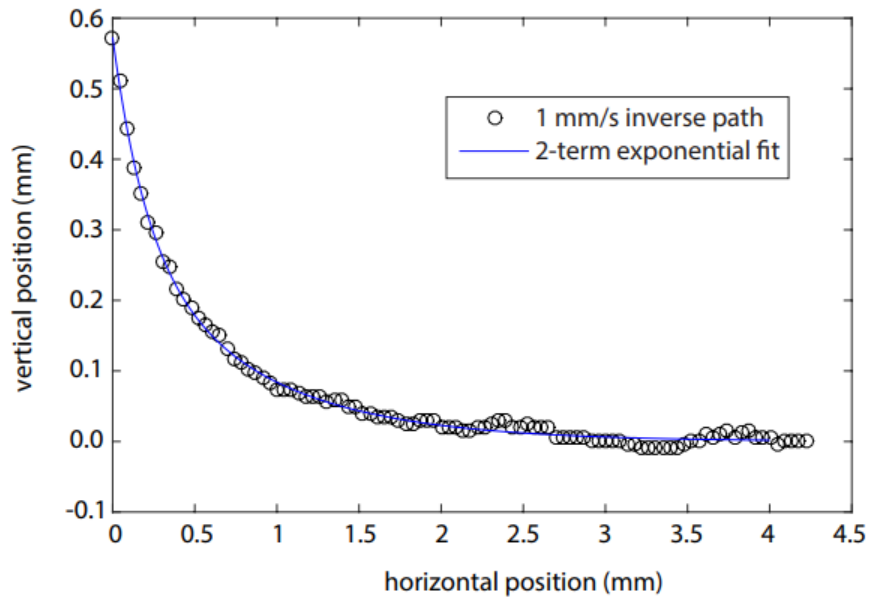


Figure 19: 2-term exponential fit to flipped average leg 2 path

## Correction Path Results

The individual and average paths of the 2<sup>nd</sup> legs printed with the full inverse correction path are shown in *Figure 20*. A clear overshoot from the desired target path is seen. Re-evaluating the full inverse correction path, the reasoning to use the flipped trajectory would only be valid if the horizontal speed while executing the trajectory of the 2<sup>nd</sup> leg was set to a constant 1 mm/s, such that it matched the horizontal speed of the original right-angle tests. The printer used is limited to a constant tangential velocity while executing a trajectory. Because the tangential velocity is set to 1 mm/s, the horizontal velocity will only be a fraction of that speed until reaching the asymptote of the correction path. The overshoot is seen at the beginning of the trajectory, where the horizontal speed is furthest from 1 mm/s.

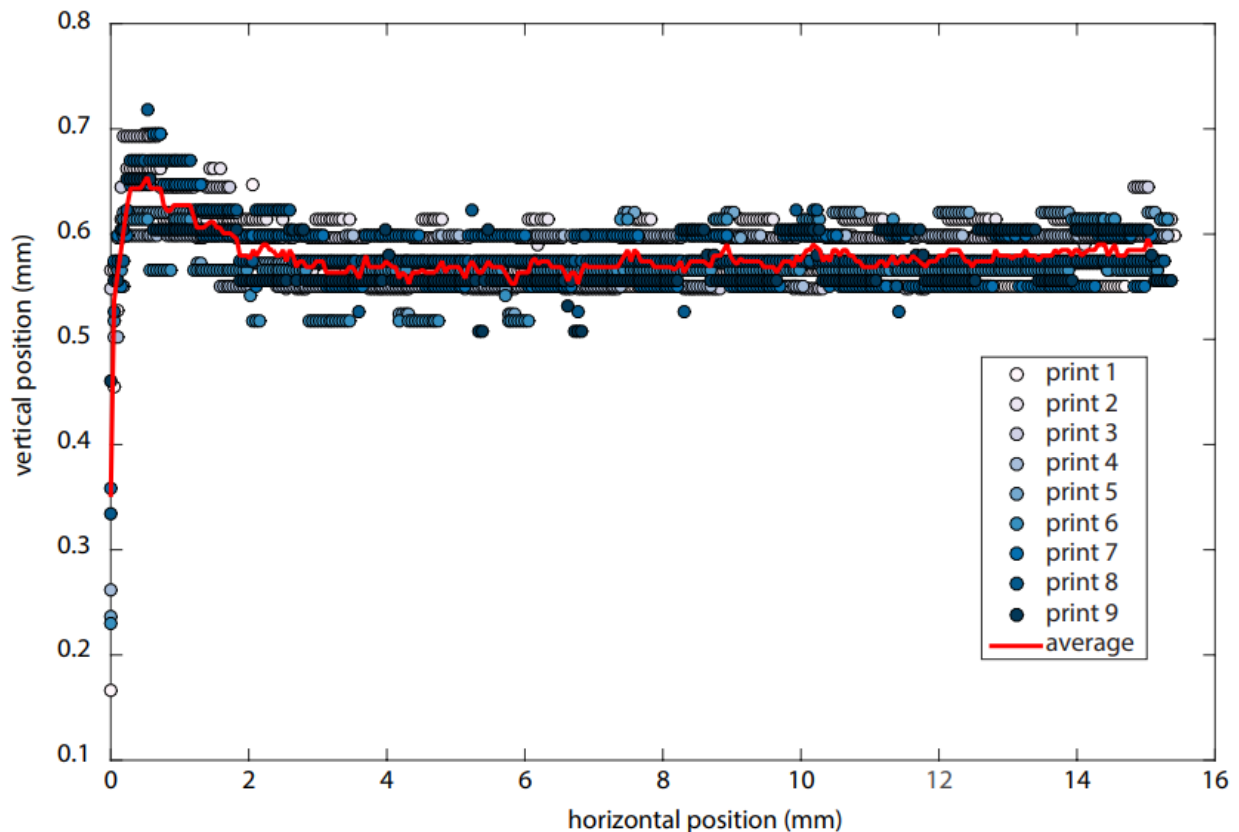


Figure 20: individual and average paths of the 2<sup>nd</sup> legs printed with the full inverse correction path

Additional correction paths are generated and tested. Similar to the full inverse correction path, 2 trajectories were created by compressing the horizontal distance of the full flipped trajectory by 75% and 50%. These new paths are referred to as the (3/4) inverse and (1/2) inverse correction paths. Two more correction paths are generated by implementing the asymptote height of the average leg 2 paths from the initial right-angle prints. The average asymptote was approximated at 0.576 mm. Referred to as the full overshoot correction path, the printer was set to move 20.576 mm in the (+)Y direction, overshooting the vertex of the target path by 0.576 mm, before moving 0.576 mm in the (-)Y direction, and then 25 mm in the (+)X direction. Referred to as the (3/4) overshoot correction path, the printer follows the same steps as the full

overshoot path, while only overshooting the target vertex by 75% of the asymptote, 0.432 mm. Each of these correction paths were tested for 5 prints. The average leg 2 paths of all corrections tests are overlaid with the results of the original right-angle path (see *Figure 21*).

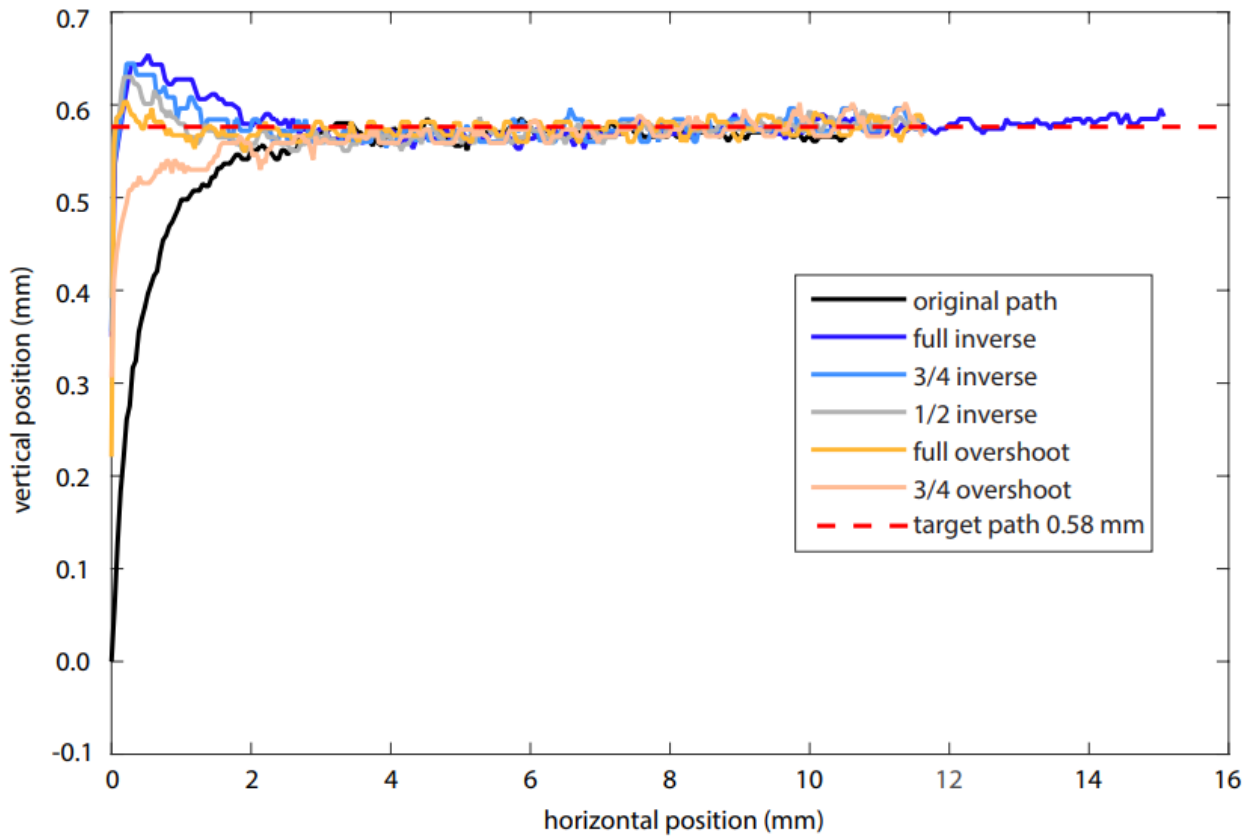


Figure 21: average needle tip paths of the 2<sup>nd</sup> legs from initial right- angle test and correction paths

The final output of the MATLAB code used to analyze the printed features shows the feature outline overlaid with the solved needle tip path. These plots showed interesting results, specifically for the full overshoot and (3/4) overshoot correction paths. Although the full overshoot correction resulted in a solved needle tip path closest to the target right angle, the outer edge of the feature had a consistent overshoot (see *Figure 24*). The (3/4) overshoot resulted in a solved needle tip path which undershot the target right angle, however, the outer edge of the feature was closest to a sharp right angle (see *Figure 24*).

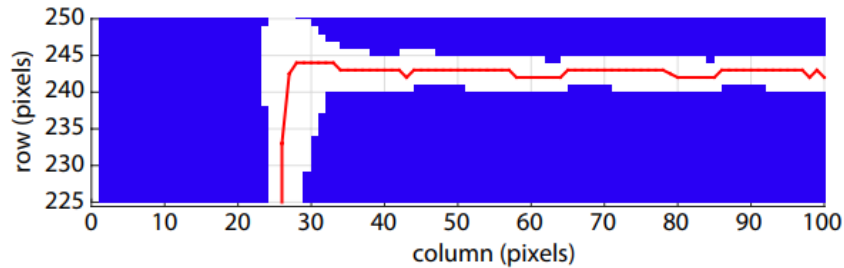
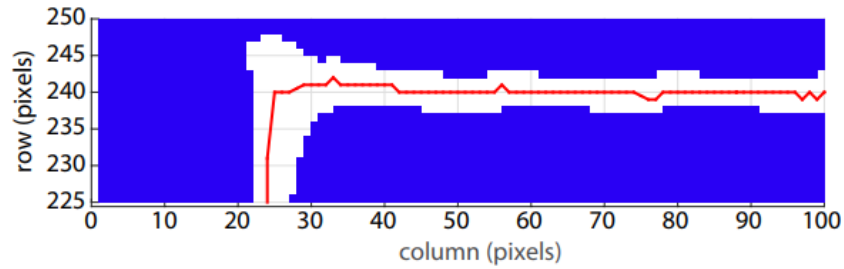


Figure 22: feature outline overlaid with solved needle tip path from full overshoot correction paths

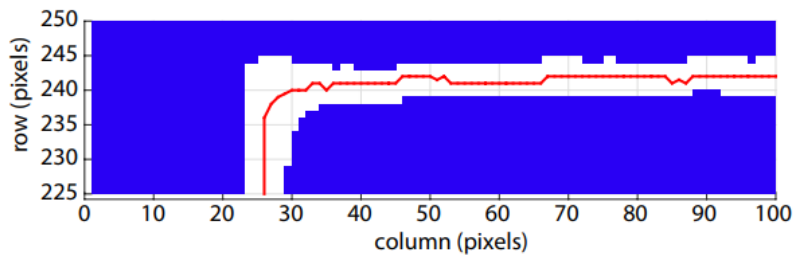
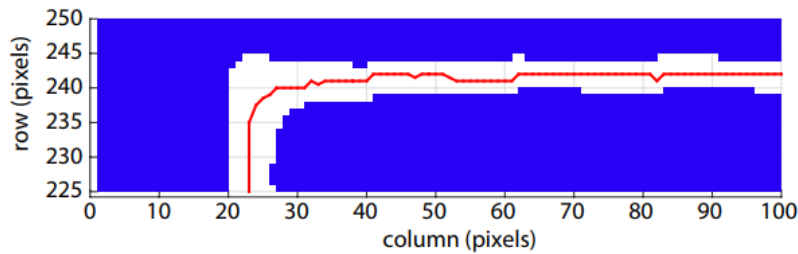


Figure 23: feature outline overlaid with solved needle tip path from (3/4) overshoot correction paths

## Rheological Measurements

Rheological measurements of the 0.2% microgel were completed using the MCR 702 Anton Paar Rheometer, with rough plates. Measurements were conducted at 25 °C, over a range of shear rates from  $500 \text{ s}^{-1}$  to  $1\text{e-}3 \text{ s}^{-1}$ . Shear rates are calculated as the ratio of printing velocity and outer diameter of the needle (Tapomoy Bhattacharjee, 2015). Rheological data was measured twice throughout this study. The first test consisted of printing at velocities 0.1, 0.3, 0.5, 1, 3, 5, 10, 30,

and 50 mm/s. 9 prints were completed at 1 mm/s and 1 print at all other velocities. Rheological data was measured 48 hours after the completion of this first test. After the conclusion of the second test measurements were taken using the same batch of 0.2% microgel. The second test consisted of printing various correction paths all at a velocity of 1 mm/s. The rheological data was measured a second time 24 hrs after the completion of the second test. Both sets of data are plotted as shear rate vs. shear stress, with corresponding cross over shear rates (see *Figure 24*).

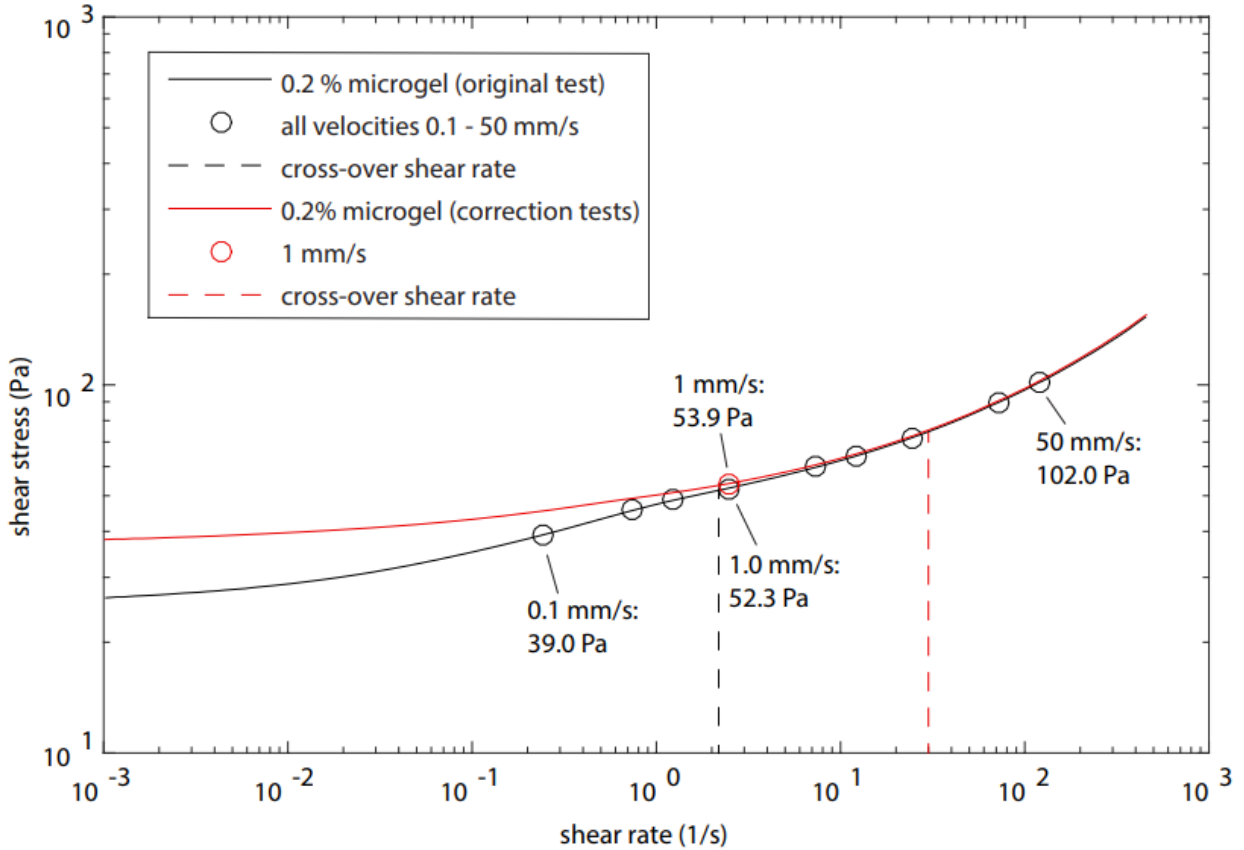


Figure 24: microgel characteristics used in testing of original right-angle path and correction paths

### Euler-Bernoulli Beam Bending Analysis

Using the rheological measurements taken, the theoretical shear rates and shear stresses for the corresponding velocities printed are compared to the deflections seen throughout this project using the Euler-Bernoulli beam bending equations. The set up of the analysis is provided in the Appendix.

Deflections of the needle tip are calculated when subject to the theoretical shear stresses of each print speed (see *Table 1*). The average asymptote height of the original right angle prints, and therefore the average needle tip deflection, is 0.576 mm (see *Figure 15*, *Figure 16*, *Figure 17*). The measured deflection is between 21 and 55 times greater than those calculated based on the theoretical stresses.

Table 1: Needle Tip Deflection for Theoretical Shear Stress

Printing Speed (mm/s)	Shear Stress (Pa)	Needle Tip Deflection (mm)
0.1	39.2	-1.05E-02
0.3	66.0	-1.76E-02
0.5	48.5	-1.30E-02
1	52.3	-1.40E-02
3	59.7	-1.59E-02
5	64.2	-1.71E-02
10	71.9	-1.92E-02
30	90.0	-2.40E-02
50	101.9	-2.72E-02

Assuming the shear stress and equivalent distributed pressure is acting on the a projected area equal to the needle tip depth in the microgel multiplied by the outer diameter of the needle, the stress required to cause a 0.576 mm tip deflection is calculated at 2,157 Pa. This is between 21 and 55 times greater than the theoretical shear stresses of each print velocity.

A final analysis is completed where the deflection of the needle tip is set to the measured 0.576 mm and the pressure acting on the needle is set to the yield stress of the microgel. The yield stress is set to 27 Pa, and is the shear stress seen at the lowest shear rates of the rheological measurements. The pressure acting on the needle is evenly distributed over an area set to the depth of needle tip multiplied by a variable width. This variable width, the hydrodynamic diameter is solved for as 32.75 mm. This hydrodynamic diameter is 80 times larger than the needles outer diameter. Even when setting the distributed pressure to the maximum theoretical stress of the range of printing speeds, 102 Pa for the 50 mm/s print, the hydrodynamic diameter solved for is 22.57 mm and 55 times the needles outer diameter.

## Discussion

Shown in *Figure 15*, *Figure 16* and *Figure 17*, the deviation of the needle tip from the printer path is seen to be independent of velocity. Not only is the undershoot of the needle tip independent of velocity, but the horizontal distance required for the needle tip to recover is also independent of velocity. This implies that the speed at which the needle tip recovers scales proportionally with velocity. Even though the print at 50 mm/s is moving 500 times faster through the 2<sup>nd</sup> leg than the print at 0.1 mm/s, the distance taken to recover is relatively constant. If there are in fact dependencies between the print velocity and undershoot distance or print velocity and recovery distance, the variations are too small to be captured by the experimental procedure used. The rheological measurements (see *Figure 24*) show that the shear rates corresponding to the print velocities tested lie on both sides of the cross over shear rate. Therefore, similar needle tip paths are seen when printing in both the solid-like characteristic and viscous fluid-like characteristic regimes of the microgel.

This raises the question of what forces are acting on the needle during each leg of the print. It is possible that multiple forces are acting on the needle in both regimes of the microgel. These forces may scale differently with velocity such that the equivalent loading of the combined forces is constant for each velocity tested.

An additional explanation raises the question of whether the velocities tested actually lie in both regimes of the microgel. It is possible the theoretical shear rates and corresponding shear stresses are not accurate. The constant deflection among velocities tested hints that the microgel is showing primarily solid like characteristics. A revised shear rate calculation with greater accuracy may show the entire range of velocities tested to lie within the solid like characteristic regime of the microgel, with minimal differences in shear stress.

### **Future Work**

The physics affecting needle bending and needle recovery can be explored further to discover physical explanations for the consistency of needle tip paths across the velocities tested. Future experiments can be completed using a similar procedure while changing other variables such as needle diameter, needle length, submerged needle tip depth, carbomer concentration of the microgel support medium, and geometry of the printed feature.

Similar experimental procedures and image analysis codes can be applied to generate correction paths for various other geometries. By iterating through various corrections paths and analyzing the results it is possible for the corresponding needle tip path to converge to the desired feature geometry.

### **Conclusions**

The experimental procedure and MATLAB code showed promise in their ability to generate correction paths that give higher precision print geometries. By quantifying the deviation of the needle tip from the desired right angle, it is possible to iterate through multiple correction paths and slowly converge to features with smaller deviations from the target path. For the range of velocities tested both the undershoot distance and recovery distance, while transitioning from the 1<sup>st</sup> to 2<sup>nd</sup> leg of the right angle are seen to be independent of velocity.

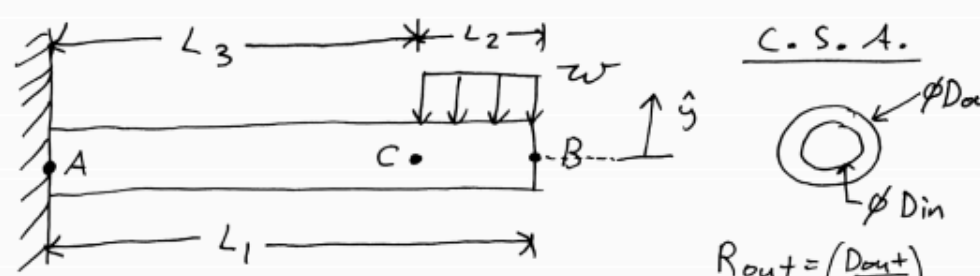
## References

- [1] Christopher S. O'Bryan, T. B. (2017). Three-dimensional printing with sacrificial materials for soft matter manufacturing. *MRS Bulletin* .
- [2] A. McGheeEmail, A. B. (2018). Full-Field Deformation Measurements in Liquid-like-Solid Granular Microgel Using Digital Image Correlation. *Experimental Mechanics* .
- [3] Tapomoy Bhattacharjee, S. M. (2015). Writing in the granular gel medium. *Materials Science* , 7.

## Appendix

### Needle Bending From Uniformly Distributed Shear Stress

\*\*The analysis is shown with and without a small angle approximation. The results of the analysis provided in this report do not incorporate the small angle approximation\*\*



Distributed load:

$$w = \tau D_{out}$$

$\tau \equiv$  shear stress

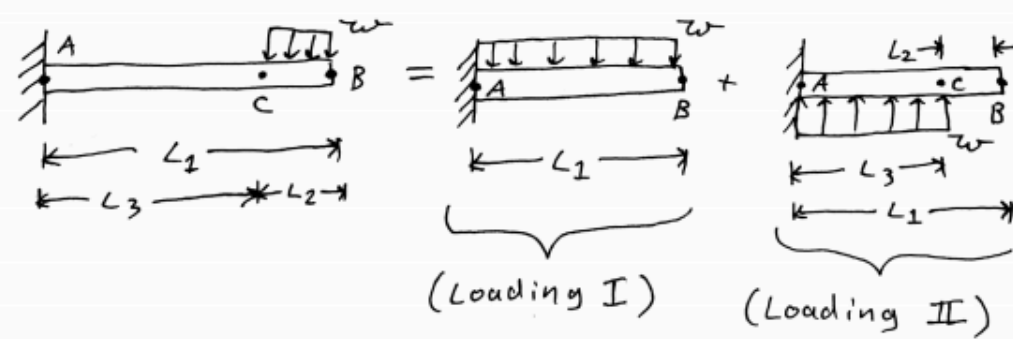
$E \equiv$  elastic modulus

$B \equiv$  needle tip       $C \equiv$  top surface of microgel

$$I = \left( \frac{\pi R_{out}^4}{4} \right) - \left( \frac{\pi R_{in}^4}{4} \right)$$

Needle tip deflection: calculated using Euler-Bernoulli Beam Bending equations (Mechanics of Materials, 6<sup>th</sup> ed, F. P. Beer, Page A28) and the Principle of Superposition.

Principle of Superposition:



$\Theta \equiv$  slope (radians)       $y \equiv$  vertical deflection

Loading I :

$$\text{Point B: } (\theta_B)_I = \frac{-w(L_1)^3}{6EI} \quad (y_B)_I = \frac{-w(L_1)^4}{8EI}$$

Loading II :

$$\text{Point C: } (\theta_C)_II = \frac{w(L_3)^3}{6EI} \quad (y_C)_II = \frac{w(L_3)^4}{8EI}$$

Point B:

$$(\theta_B)_II = (\theta_C)_II \quad (y_B)_II = (y_C)_II + \overbrace{[(\theta_C)_II (L_2)]}^{\text{small angle approximation}}$$

Total deflection at B : (tip deflection)

$$y_B = (y_B)_I + (y_B)_II$$

Large Angles :

for larger angles the small angle approximation is no longer valid and the equation

for  $(y_B)_II$  becomes :

$$(y_B)_II = (y_C)_II + [\sin(\theta_{CII})(L_2)]$$